ACS APPLIED MATERIALS & INTERFACES

Research Article

www.acsami.org

Scalable Preparation of Ultrathin Silica-Coated Ag Nanoparticles for SERS Application

Yanjie Hu,[†] Yunli Shi,[†] Hao Jiang,[†] Guangjian Huang,[‡] and Chunzhong Li*[,†]

[†]Key Laboratory for Ultrafine Materials of Ministry of Education, School of Materials Science and Engineering, East China University of Science & Technology, Shanghai 200237, China

[‡]Department of Surgery, Huashan Hospital, Fudan University, Shanghai 200040, China

ABSTRACT: Silica-coated Ag nanoparticles (Ag@SiO_2 NPs) have been successfully prepared by a scalable flame spray pyrolysis (FSP) technique with production rate up to 4 g/h in laboratory-scale. The ultrathin SiO_2 shell, with a thickness 1 nm, not only effectively avoids the intersintering of Ag nanoparticles core at the high temperature, but also serves as a protective layer of the SERS-active nanostructure. The silica-coated Ag nanoparticles form agglomerates in the large temperature gradient zone, which with several nanometers gaps from each other but not contact. Such an intriguing feature can result in more Raman hot-spots generated at the gaps among Ag core active sites, which will beneficial for the whole SERS substrate enhancement. The results demonstrate that a maximum enhancement factor can reach ~10^5 with a detectable concentration as low as 10^{-10} M for rhodamine 6G (R6G) molecules, indicating that the as-obtained unique nanostructure will be a promising candidate for SERS applications.

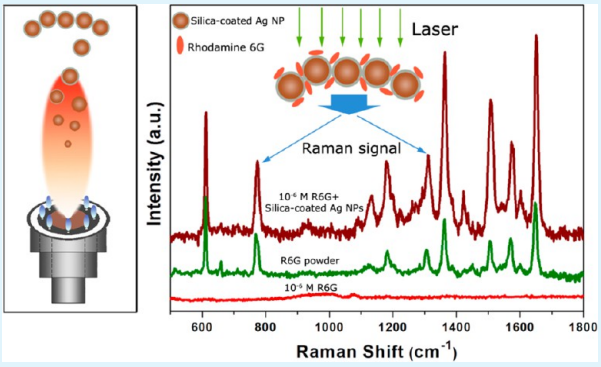

KEYWORDS: *ultrathin silica-coated, Ag@SiO_2 NPs, FSP, SERS*

1. INTRODUCTION

Flame spray pyrolysis (FSP) is a powerful route that can dissolve the precursor directly in the fuel, simplicity of introduction of the precursor into the flame reaction zone, and flexibility in using the high-velocity spray jet for rapid quenching of aerosol formation.[1] Compared with the chemical method, FSP methods have the advantages of one-step, rapid, continuous synthesis for nanomaterials, which is very important for scale-up preparation.[2,3] Actually, the energy consumption is also low due to the rapid synthesis process, about microsecond levels. As for the chemical method, a complicated process is needed including washing, filtration, drying and so forth, which is time-consuming process. In addition, more steps often suggest lower yield and higher cost. In addition, by FSP methods, many materials with various nanostructures, such as 1D nanowires,[4] 2D nanosheets[5] and even complex 3D configurations,[6] can also be realized. It is noted that amounts of composites can also been synthesized by this method, such as TiO_2@SnO_2,[7] Fe_2O_3@SiO_2,[8] Y_2O_3@SiO_2[9], and other core–shell structures.[10] A depth understanding for flame combustion process will be beneficial for guiding the production of novel nanomaterials with amounts of functionalities.

Surface-enhanced Raman scattering (SERS), a powerful spectroscopic technique, has attracted much attention since its discovery in the 1970s.[11] The obtained enhanced Raman signals facilitate the precise and convenient identification of fingerprint signatures of molecules in chemical and biological systems, showing wide applications in many fields such as analytical chemistry, life and environment science.[12−15] In the past decade, various efforts have been made to prepare effective SERS active materials. For example, multiparticles assemblies of nanoscale structures enable the formation of the complex nanoplasmonic structures with subnanometer gaps between prepared noble metal materials, such as Ag nanoparticles dimers,[16] polygonal nanofinger Au assemblies[17] and self-assembled chains of Au nanorods.[18] These efforts have been done for increasing the so-called "hot spots" by enhanced localized surfaced plasmonic resonances. The maximum enhancement factor may be as high as 10^{11}or even more.[17] This makes the single molecules surface enhanced Raman spectroscopy analysis become possible.

However, Raman signals of some reported molecules adsorbed on the hot-spots region may be changed because of the Plasmon effect or catalysis activity of noble metal,[19] which limits the SERS technique for further qualitative analysis.[20,21] Tian and Wang et al.[22] have developed a novel shell-isolated nanoparticle-enhanced Raman spectroscopy technique, in which gold nanoparticles encapsulated by an ultrafine and chemically inert silica or alumina shell. The inert shells with several nanometers can effectively prevent the probed molecules from directly adsorbing on the SERS-active site and vast practical application to various probed molecules.

Received: July 2, 2013
Accepted: October 11, 2013
Published: October 11, 2013

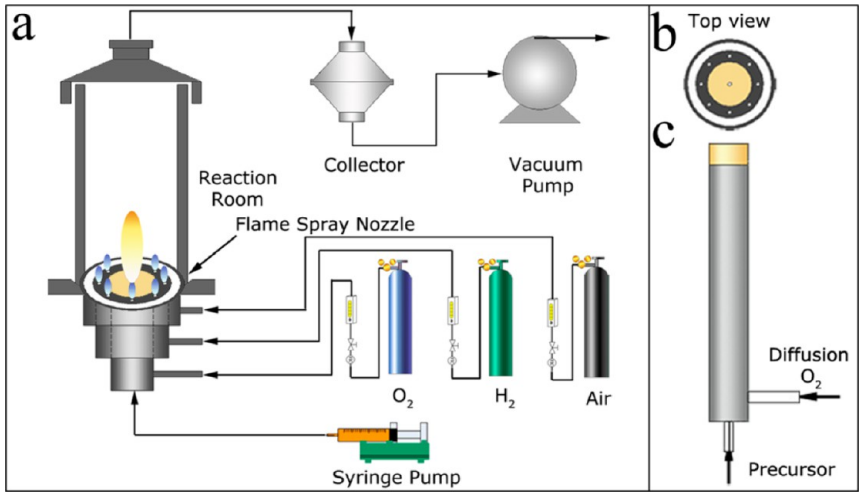

Figure 1. (a) Schematic of the FSP setup for preparing silica-coated Ag nanoparticles, (b) top view of FSP nozzle, and (c) schematic of the spray nozzle.

Herein, we introduce a rapid, scalable FSP technique to realize the preparation of Ag@SiO_2 nanoparticles by introduce of mixture precursors (silver nitrate and tetraethyl orthosilicate) ethanol solutions into hydrogen/air flame reaction zone. The hydrogen/air flame was chosen to receive adequate temperature for obtaining dense and homogeneous fine particles which have diameters of ~30 nm and are coated by ultrathin silica. The as-prepared materials could be good candidate for Surface-enhanced Raman scattering active substrate. The as-prepared ultrathin silica-coated Ag nanoparticles were proven to be without any naked or pinholes on the surface, which can be seem as shell-isolated nanoparticles. Application of as-prepared nanoparticles as SERS active materials for detecting of R6G molecules, the results indicated that they possess a high sensitivity and low detection limit.

2. EXPERIMENTAL SECTION

2.1. Reagents and Materials. Silver nitrate ($AgNO_3$, AR), tetraethyl orthosilicate (TEOS, AR) and ethanol were purchased from Sinopharm chemical reagent Co. Ltd. Hydrogen (H_2) and Oxygen (O_2) were purchased from Siling gas Co. Ltd. 4-mercaptobenzoic acid (4-MBA, AR) was purchased from Shanghai Hansi Co. Ltd. Glass filters (GA 55) were purchased from Toyo Roshi Kaisha, Ltd. All chemicals were used as received.

2.2. FSP Synthesis of the Silica-Coated Ag Nanoparticles. The silica-coated Ag nanoparticles were synthesized by introducing a precursor solution of silica and silver into a closed FSP reaction zone, in which a hydrogen/air diffusion flame was used as supporting flame and heat source. Figure 1 presents a detailed description of the FSP setup, including a precursor delivery unit, a flame spray nozzle, a reaction room and powder collection unit. The flame spray nozzle is composed of two sections, which is shown in Figure 1b and c. One is the two-concentric steel rings where air is fed through the first ring (from outer to inner) and the hydrogen is supplied from the second one with eight pores of 1 mm in diameter. And another is a typically oxygen-supported spray nozzle, in which a steel capillary with an inner diameter of 0.6 mm is fixed in the central. The dispersed gas was introduced through the interspace of the spray nozzle and the capillary. The precursor mixture solutions were fed at 3 mL/min through the capillary and dispersed by 5 L/min oxygen forming the ultrafine droplets. Then droplets were ignited by a diffusion hydrogen/air flame (2/25 L/min), which not only served as supporting flames, but also afforded additional thermal energy to melting/decomposition of the precursor with low combustion enthalpy. In detail, as for the Ag@SiO_2 synthesis, a predetermined amount of TEOS was added to obtain the desired silica content while the concentration of silver nitrate was designed at 0.2 M. We assumed that all precursors of Ag and Si formed the product Ag and silica. The weight fraction of silica in the product nanparticles was defined as

$$\text{wt \%SiO}_2 = \frac{\text{mass}(SiO_2)}{\text{mass}(SiO_2) + \text{mass}(Ag)} \times 100 \quad (1)$$

The wt % SiO_2 was range from 0.5 to 15 wt %. The spray droplets underwent solvent evaporation, combustion, pyrolysis of TEOS and silver nitrate, nucleation growth, aggregation or agglomeration growth in a short flame process, and eventually formed the as-prepared products. The flame made powders were collected on a glass filter in the collector chamber with the aid of a vacuum pump.

2.3. Particles Characterization. Transmission electron microscope (TEM) image, high resolution transmission electron microscope images and EDS pattern of the sample were taken by JEM 2010 and JEM 2100 equipped with an energy-dispersive X-ray spectroscopy (EDS). The corresponding X-ray diffraction pattern was conducted by a Rigaku D/max 2550VB/PC diffractometer over a 2θ range of 20–80° at an angular resolution of 0.02°. UV–visible spectra of aqueous dispersions of the obtained samples were recorded on a UV–vis spectrophotometer using a 1 cm quartz cell.

2.4. Measurements of SERS Activity of Ag@SiO_2 NPs. Raman spectra were recorded on a Laser in-Via Raman microprobe system (inVia-Reflex, Renishaw Instruments, England), equipped with Peltier charge-coupled device (CCD) detectors and a Leica microscope. The as-prepared nanoparticles were used as SERS active materials to detect R6G molecules with different concentrations. Briefly, 1 mM R6G solution in ethanol was prepared and diluted with ethanol to predetermined concentrations. And then, 1 mg of as-prepared samples added to the 2 mL of the different concentration R6G solutions in a centrifuge tube, followed by shaking for 5 min. The mixture was evenly coated on a glass and then dried at room temperature for SERS measurement. Samples were excited with a 514 nm laser line. Spectra were collected in Renishaw continuous mode with accumulation times of 10 s. The laser power was set to 1% of the full power (30 mW). The laser beam was focused on the sample in backscattering geometry using a 10× objective providing scattering areas of ~3 μm in diameter.

2.5. Calculation of the Enhance Factor (EF). To estimate the SERS abilities of the as-prepared silica-coated Ag NPs, we compare the intensity of the peak at 1652 cm^{-1} of 10^{-6} M R6G with the spectra of R6G powders and calculate the enhance factor (EF)[23,24] according to the equation

$$EF = \frac{I_{SERS}/N_{SERS}}{I_{BULK}/N_{SERS}} \quad (2)$$

where I_{SERS} denotes the SERS intensity of the 1652 cm^{-1} band of R6G adsorbed on the as-prepared substrate. I_{Bulk} denotes the normal Raman scattering intensity of the same band of pure R6G powder, and N_{SERS} and N_{Bulk} are the number of R6G molecules effectively excited by the laser beam to get the corresponding SERS and bulk spectra, respectively.[25]

2.6. Detection of Pinholes for Ag@SiO_2 NPs. 4-MBA molecules are employed as the detected molecule because of its sulfhydryl group, which could strongly chemisorbed onto the surfaces of Ag NPs. Specifically, 1 mg as-prepared Ag@SiO_2 Nps were put into 1 mL ethanol solution of 4-MBA (10^{-3} mol/L) for 24 h, washed 5 times with ethanol in an ultrasonic conditions, and then dried at room temperature for SERS measurement.

3. RESULTS AND DISCUSSION

The silica-coated Ag nanoparticles have been obtained via flame copyrolysis of the corresponding precursors of silver and silica. Figure 2 shows the XRD pattern of the prepared nanoparticles

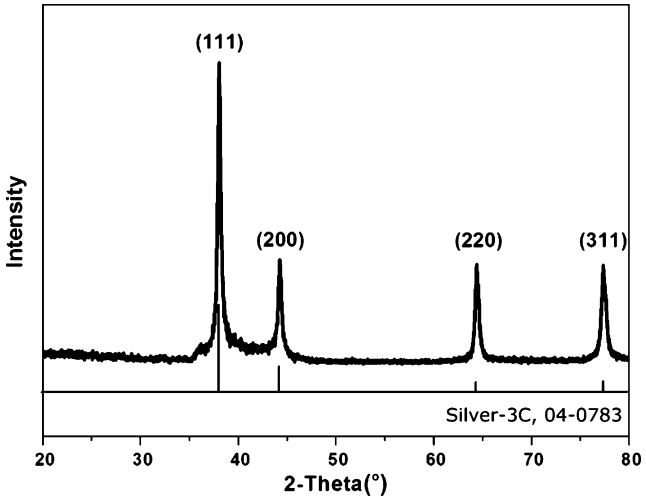

Figure 2. XRD pattern of the as-prepared ultrathin silica-coated Ag nanoparticles with 5 wt % of silica.

with 5% SiO_2. The diffraction peaks are clearly observed at 2θ values of 38.1°, 44.3°, 64.5°, and 77.4°, which can be indexed to the (111), (200), (220), (311) crystal planes of silver nanoparticles (Silver-3C, JCPDS No. 04-0783). It is noted that there is no trace of silica due to the low content (5%) or the bulk amorphous nature. Furthermore, no peaks of Ag_2O can be observed in the XRD pattern, which may be attributed to the low decomposition temperature (300 °C) of Ag_2O and high temperature (above 1500 °C) of H_2/air diffusion flame. Therefore, metallic Ag nanoparticles have been obtained by a typical FSP technique.

TEM images of the as prepared ultrathin silica-coated nanoparticles with the silica content of 5 wt % are presented in Figure 3a. It can be confirmed that the highly crystalline nanoparticles with an average diameter of ~30 nm show a nearly spherical shape. The as prepared nanopartilces were aggregated but not sintered from each other. This can also be verified by Figure 3b, in which a continuous SiO_2 layer with a thickness of about 1 nm has been observed on the surface of every Ag cores. Then the formed silica-coated Ag nanoparticles aggregated from each other to an aggregation. Therefore, these silica layers prohibit the further sintering of the Ag cores and as a ligand to link every as-made nanoparticles forming aggregations. Between two adjacent core−shell NPs, there are tiny gaps with a width of 1−4 nm, which are composed of inert amorphous SiO_2.

Figure 3c shows the high resolution TEM image of silica-coated nanoparticle. The clear lattice fringes are also observed, indicating the high crystalline feature of Ag cores. The corresponding interplanar spacing of 0.103 nm is in good agreement with the distance of the (400) plane of metallic silver. Between two adjacent silica-coated Ag nanoparticles, there are tiny gaps with a width of 1−4 nm, which are composed of inert amorphous SiO_2. Figure 3d shows the corresponding EDS pattern of the flame made ultrathin silica-coated Ag nanoparticles, indicating that the main components of the sample are Ag, Si, and O with a weight ratio of 38.2: 0.93: 1.

The chemical and physical reaction of gases, precursors and solution in the high temperature reaction zone is drastic and only lasts for a few milliseconds. Therefore, the particle formation mechanism is always a "black box". In present, there are two mechanisms have been proposed to explain the coating formation during the coflame synthesis of silica with other materials. The important one is the different reaction rates of different precursors, which has been reported to explain the formation mechanism of the TiO_2/SiO_2 core−shell structures[7] and the SiO_2-coated $BiVO_4$ nanoparticels.[21] According to this mechanism, the Ag vapor is formed first from silver nitrate whose decomposition point is only 440 °C ($2AgNO_3 = 2Ag + 2NO_2 + O_2$). After the process of collision/coalescence,[1] the Ag nanoparticles nucleate to larger ones then a silica coating forming on the Ag nanoparticles surface in the downstream. At the last stage, the silica-coated Ag nanoparticles self-assemble into aggregations due to temperature gradient in the reaction zone. Another feasible mechanism has been proposed to illustrate the Fe_2O_3/SiO_2 and ZnO/SiO_2 formation process.[22] In the high temperature reaction zone, the mixture of precursors underwent decomposition process into gas-phase Si, O and metal species. In the downstream of flow direction, the condensation of gaseous species generates the molten or liquid metal oxides, due to the decreasing of flame temperature. The immiscibility of the two liquid species and high mobility at the high temperatures leads to phase segregation prior to solidification of the particle. The driving force for segregation is reduction free energy of the system by formation of thermodynamically favored phase. Therefore, difference surface energy then could lead to continuous silica on the surface of metal/metal oxides nanoparticles during solidification.

To further investigate the effect of SiO_2 on the structure and distribution of Ag nanoparticles, the Ag/SiO_2 nanocomposites with different SiO_2 content (0.5−7 wt %) were designed and prepared by FSP method simply change the content of the TEOS in the precursors. The corresponding TEM and size distribution images are shown in Figures 4 and 5. The obtained Ag/SiO_2 (weight ratio of SiO_2 = 0.5 wt %) nanoparticles show clearly sintering necks because of high flame temperature, with very small trace of TEOS in the precursor solution, as shown in Figure 4a. More interestingly, the sintering among silver particles disappeared gradually and the average diameter of the as-prepared nanoparticles is monotonous decreased obviously with increase SiO_2 weight ratio. In the fast temperature gradient reaction zone, silica act as a barrier and prevent the Ag nanoparticles from coalescence into larger particles and the spontaneously formed silica coating prevents the sintering of the Ag nanoparticles. Therefore, the amorphous silica not only serves as a barrier to impede the nanoparticle from sintering

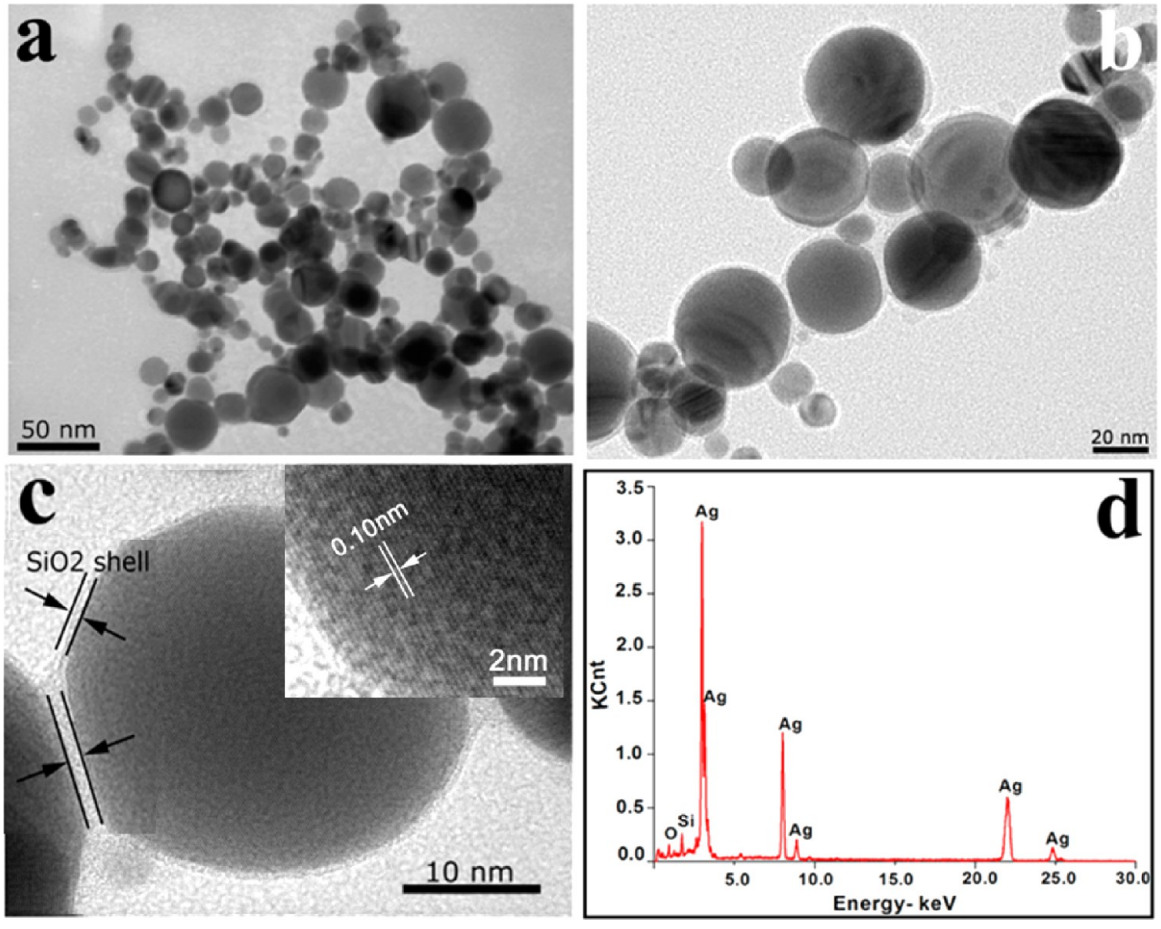

Figure 3. (a) TEM, (b) High-magnification, (c) high-resolution TEM images, and (d) EDS pattern of the as-prepared ultrathin silica-coated Ag nanoparticles.

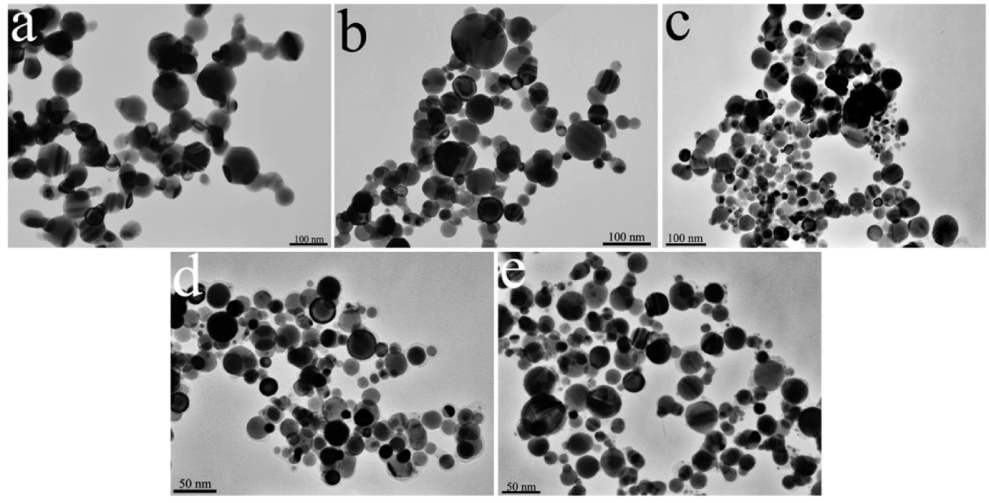

Figure 4. TEM images of silica-coated Ag nanoparticles with different content of silica: (a) 0.5, (b) 1, (c) 3, (d) 5, and (e) 7 wt %.

into each other, but also prevents the Ag nanoparticle growing in to larger one. When the weight ratio of SiO_2 was adjusted to 5 wt. %, Ag nanoparticles encapsulate with amorphous silica present a perfect core shell structure. Figure 6 shows the UV–vis absorbance spectra of Ag/SiO_2 NPs with different SiO_2 content (0.5, 1, 3, 5, and 7 wt %) in aqueous suspensions. As shown in Figure 4, the insert photo indicates that the color of the aqueous suspension gradually changes from gray to yellow with increasing of SiO_2 content. Besides, all samples have clearly peaks around 400 nm, which is dominated by the Ag components. The absorption bands are thinner with the introduction of more SiO_2. This also indicates that the optical properties of Ag particles are influenced by the presence of SiO_2, which mainly changes the interface properties between Ag particles and the surrounding medium.

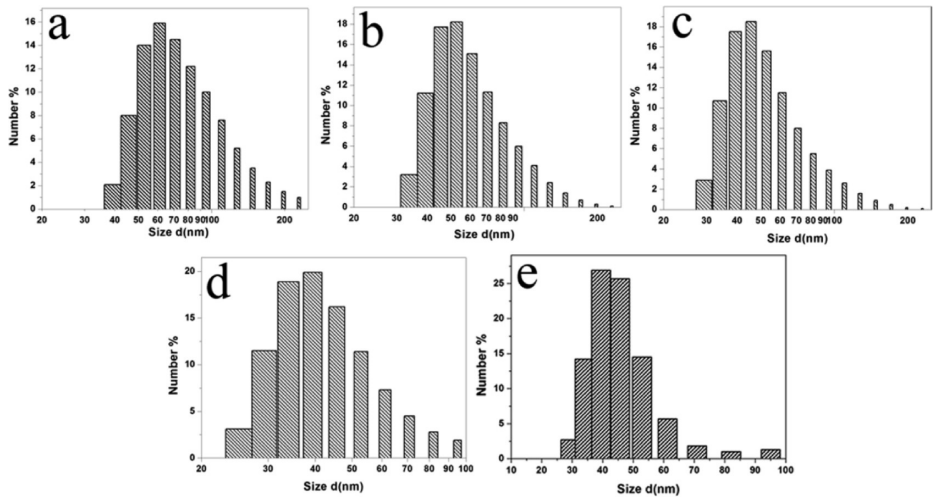

Figure 5. Corresponding size distribution of the silica-coated Ag nanoparticles with different content of silica: (a) 0.5, (b) 1, (c) 3, (d) 5, and (e) 7 wt %.

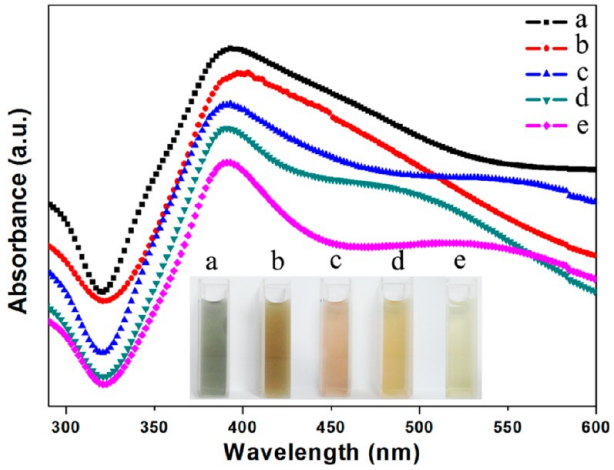

Figure 6. UV−vis absorbance spectra of Ag/SiO_2 nanocomposites with different content of silica: (a) 0.5, (b) 1, (c) 3, (d) 5, and (e) 7 wt %. Bottom insert: Corresponding photograph of the suspensions of as-made silica-coated Ag NPs.

From the above analysis, SiO_2 plays an important role in preventing the Ag cores from sintering and being used as a ligament to connect the building blocks to a chain. On the other hand, according to shell-isolated nanoparticle-enhanced Raman spectroscopy model,[26] the ultrathin SiO_2 shell can protect the detected molecules with no contact with the active Ag cores. Therefore, the ultrathin shell must be pinhole-free, or the pinhole at least smaller than the detected objectives. It is commonly known that SERS efficiency attenuates exponentially with increasing distance between the adsorbed molecules and noble metal core. To effectively transfer the strong electromagnetic field from noble metal core to the probed objective surface, pinhole-free silica-coated Ag NPs with the thinner shell the better.

Therefore, we adopt a SERS measurement to measure the flame made Ag/SiO_2 nanocomposites with different SiO_2 content whether with pinholes or not. Figure 7 shows Raman spectra of 4-MBA molecules adsorbed on the obtained Ag/SiO_2 NPs with different silica content. The left graph in Figure 7 is the schematic illustration of pinhole detention. 4-MBA molecules are employed as the detected molecule because of

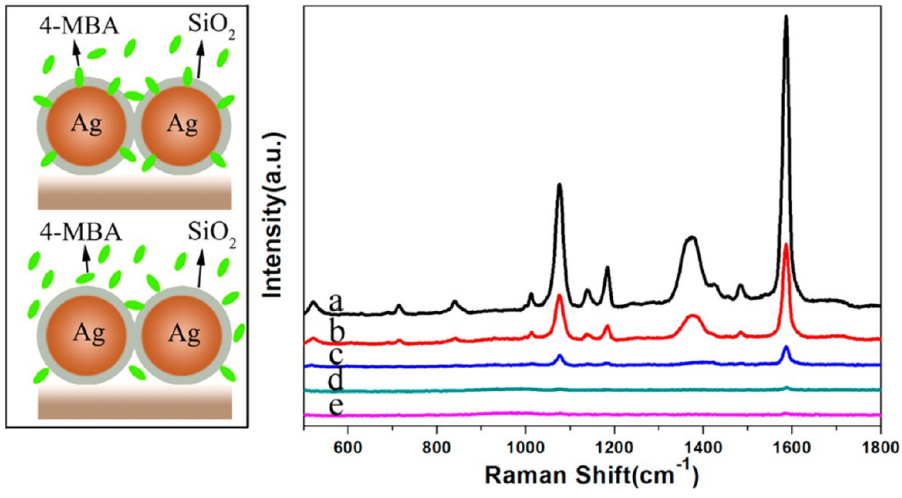

Figure 7. (a−e) Raman spectra of 4-MBA molecules adsorbed on the flame made $Ag@SiO_2$ NPs with different silica content (a−e 0.5%, 1%, 3%, 5%, and 7%, respecitively). (Left is the schematic illustration of pinhole detention.)

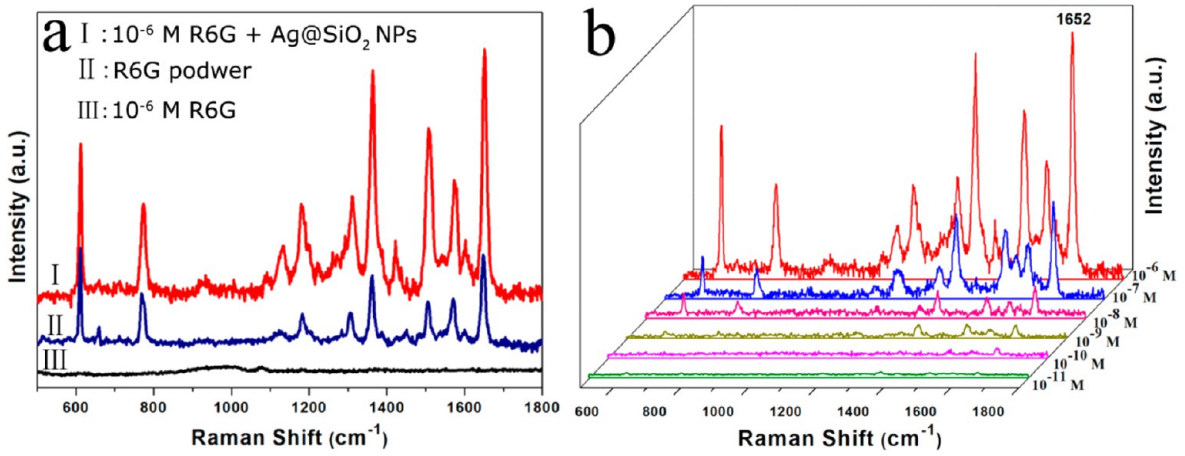

Figure 8. (a) Raman spectra of pure R6G powder and R6G molecules with the concentration of 10^{-6} mol/L adsorbed on and without 5 wt % silica-coated Ag nanoparticles. (b) Raman scattering spectra of different concentration of R6G physisorbed on 5 wt % silica-coated Ag nanoparticles.

its sulfhydryl group which could strongly chemisorbed onto the surfaces of Ag NPs. If Ag cores are not completely coated or have some pinholes, the small 4-MBA molecule might directly adsorb onto the Ag NPs surfaces though pinholes. As shown in Figure 7, the difference of the Raman scattering intensity of 4-MBA could be observed clearly. When the SiO_2 content varies from 0.5% to 3%, the Raman signals of 4-MBA molecules significantly change. In contrary, the typical Raman signals are disappeared when increase the proportion of SiO_2 to 5% or even more. It is noted that if the Ag NPs are uniform coated without pinholes or the pinholes smaller than 4-MBA, any 4-MBA that may be physisorbed onto the silica shells should be washed out by sonication and solvent washes. Therefore, we can conclude that the prepared Ag/SiO_2 nanocomposites with 5% SiO_2 are pinholes-free owing to the perfect ultrathin SiO_2 shell encapsulation on the surface of Ag cores, which could be a promising candidate for SERS application.

The SERS activity of the ultrathin silica-coated Ag NPs was tested by R6G molecules, as shown in Figure 8. All fluorescence backgrounds which generate in Raman spectroscopy of R6G molecules excited at 514.5 nm were subtracted. The main Raman bands at 611, 771, 1192, 1315, 1513, and 1652 cm^{-1} are typical peaks of R6G molecules. In Figure 8a, the Raman signals of R6G are significantly enhanced that the Raman peaks of 10^{-6} M solution of R6G are even much higher than that of R6G powders. This may be attributed to the Raman enhancement effect of the employed SERS active Ag materials. Moreover, the Raman spectra of 10^{-6} M solution of R6G molecules without adsorbed on as-prepared structure is recorded, but there is hardly Raman peaks can be distinguished. Figure 8b shows the concentration-dependent SERS spectra of R6B mode molecules with typical aromatic ring vibrations, for example, 611, 771, 1192, 1315, 1513, and 1652 cm^{-1}. Low concentration (10^{-10} M) of R6G in solution can be detected apparently. Accordingly, the as-prepared NPs with a benign nanothin silica shell may also be promising in the relatively quantitative detection of biomolecules in organisms with the advantages of simplicity and sensitivity.

To investigate the effect of content of silica in the as-made nanoparticles on the SERS activity, different weight content silica-coated Ag nanoparticles were used to detect 10^{-6} mol/L R6G molecules under the same condition. The results revealed in figure 9 show that the enhancement effect of silica-coated Ag NPs is closely related to the content of silica. When the weight

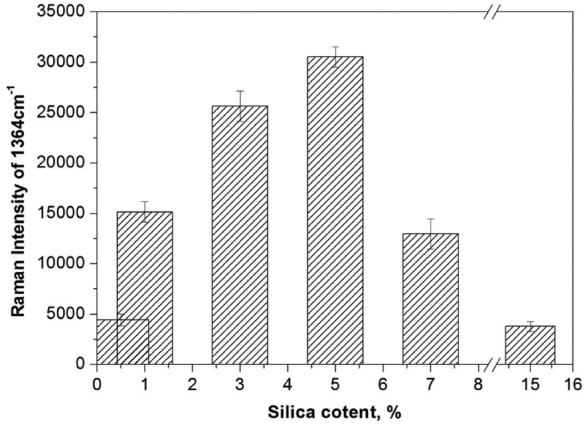

Figure 9. Variation of R6G Raman intensity (at 1364 cm^{-1}) with different content of silica-coated Ag nanoparticles (R6G concentration is 1×10^{-6} mol/L, other conditions are same).

content of silica is below 5 wt %, the enhancement effect significantly increases with the silica content. This may be contribute to the sintering of the Ag nanoparticles, for which the gaps among the particles is less than these particles with well dispersity such as silica-coated Ag NPs with 5 and 7 wt.% silica. According to SERS enhance mechanism, the enhancement of SERE active substrate mainly from the hot spots which are formed at the gap region between two Ag nanoparticles or the sharp surface of nanostructures.[27] The further increase in silica content leads to decrease of enhancement effect, which because of the SERS efficiency exponentially decreases with increasing distance between the probed molecules and Ag nanoparticle surface, this distance, namely, the thickness of the silica shell.[22]

It is assumed that the obtained sampling volume is the product of the area of the laser spot (~1 μm in diameter) and the penetration depth (~ 2 μm) of the focused laser beam. It is noted that the R6G molecular weight is 479.01 g mol^{-1}, and its density is 0.79 g/cm^3. The total number of R6G molecules which been effectively excited by the laser beam are calculated to be 1.036×10^{-14} mol. On the other hand, 20 μL solution of 10^{-6} M R6G are spread uniformly on the glass slide with an area of about 2.7 cm^2. Therefore, the total number of molecules sampled in the SERS experiment using the silica-coated Ag nanoparticles as SERS active materials would be 2.326×10^{-19}

mol. On the basis of the calculation, a monolayer of R6G molecules adsorbed on the SERS active powders is assumed. The intensity ratio of the 1652 cm^{-1} band in Figure 8a is measured to be 2.12, and the EF is estimated to 9.3×10^4 for R6G molecules from the silica-coated nanoparticles.[28]

4. CONCLUSION

In summary, we report a scalable flame spray pyrolysis (FSP) method for the synthesis of the Silica-coated Ag nanoparticles, which exhibit an excellent shell-isolated effect and good SERS effect. Due to the high temperature reaction zone and large temperature gradient, Ag nanoparticles are formed with an ultrathin silica shell. Pinhole detection shows that as-prepared NPs are free of pinholes even the silica content is 5 wt %. The ultrathin silica shell (~1 nm) not only serves as a protective layer to prevent particles from sintering but also applies as an isolator for shell-isolated nanoparticles. More significantly, a lot of hot spots can be generated between gap regions of nanoparticles of agglomerates, which exhibit an enhancement ability of SERS for R6G with the detection limit as low as 10^{-10} M. The average enhancement factor nearly about 10^5 for the band at 1652 cm^{-1}. Accordingly, it is reckoned that the as-prepared unique nanostructures with benign and sensitive properties may possess a huge potential for applications in biomedicine and quantitative analysis.

AUTHOR INFORMATION

Corresponding Author

*Tel: +86-21-64250949. Fax: +86-21-64250624. E-mail: czli@ecust.edu.cn.

Notes

The authors declare no competing financial interest.

ACKNOWLEDGMENTS

This work was supported by the National Natural Science Foundation of China (20925621, 21236003, 81071994), the Shanghai Rising-Star Program (13QA1401100), the Special Projects for Nanotechnology of Shanghai (11 nm0500800, 11 nm0500200), the Basic Research Program of Shanghai (11JC1403000), the Special Research Fund for the Docoral Program of Higher Education of China (20110074110010), and the Fundamental Research Funds for the Central Universities.

REFERENCES

(1) Teoh, W. Y.; Amal, R.; Mädler, L. *Nanoscale* **2010**, *2*, 1324−1334.
(2) Sotiriou, G. A.; Sannomiya, T.; Teleki, A.; Krumeich, F.; Vörös, J.; Pratsinis, S. E. *Adv. Funct. Mater.* **2010**, *20*, 4250−4257.
(3) Tricoli, A.; Righettoni, M.; Teleki, A. *Angew. Chem., Int. Ed.* **2010**, *49*, 7632−7659.
(4) Liu, J.; Gu, F.; Hu, Y. J.; Li, C. Z. *J. Phys. Chem. C* **2010**, *114*, 5867−5871.
(5) Hu, Y. J.; Xu, K. X.; Jiang, H.; Li, C. Z. *Chem. Eng. J.* **2013**, DOI: 10.1016/j.cej.2013.09.054.
(6) Liu, J.; Hu, Y. J.; Li, C. Z. *Ind. Eng. Chem. Res.* **2009**, *48*, 735−739.
(7) Li, Y. F.; Hu, Y. J.; Jiang, H.; Li, C. Z. *RSC Adv.* **2013**, DOI: 10.1039/C3RA44629H.
(8) Li, Y. F.; Hu, Y. J.; Jiang, H.; Li, C. Z. *Nanoscale.* **2013**, *5*, 5360−5367.
(9) Sotiriou, G. A.; Franco, D.; Poulikakos, D.; Ferrari, A. *ACS Nano* **2012**, *6*, 3888−3897.
(10) Teoh, W. Y.; Amala, R.; Mädler, L. *Nanoscale* **2010**, *2*, 1324−1347.
(11) Fleischmann, M.; Hendra, P. J.; McQuillan, A. *J. Chem. Phys. Lett.* **1974**, *26*, 163−166.
(12) Fan, M.; Andrade, G. F. S.; Brolo, A. G. *Anal. Chim. Acta* **2011**, *693*, 7−25.
(13) Wachsmann-Hogiu, S.; Weeks, T.; Huser, T. *Curr. Opin. Biotechnol.* **2009**, *20*, 63−73.
(14) Graham, D.; Goodacre, R. *Chem. Soc. Rev.* **2008**, *37*, 883−884.
(15) Kasim, J.; Tee, X. Y.; You, Y. M.; Ni, Z. H.; Setiawan, Y.; Lee, P. S.; Chan, L.; Shen, Z. X. *J. Raman Spectrosc.* **2008**, *39*, 1338−1342.
(16) Stranahan, S. M.; Titus, E. J.; Willets, K. A. *ACS Nano* **2012**, *6* (2), 1806−1813.
(17) Ou, F. S.; Hu, M.; Naumov, I.; Kim, A.; Wu, W.; Bratkovsky, A. M.; Li, X.; Williams, R. S.; Li, Z. *Nano Lett.* **2011**, *11*, 2538−2542.
(18) Lee, A.; Andrade, G. F. S.; Ahmed, A.; Souza, M. L.; Coombs, N.; Tumarkin, E.; Liu, K.; Gordon, R.; Brolo, A. G.; Kumacheva, E. *J. Am. Chem. Soc.* **2011**, *133*, 7563−7570.
(19) Yang, W. R.; Liu, J. Q.; Zheng, R. K.; Liu, Z. W.; Dai, Y.; Chen, G. N.; Ringer, S.; Braet, F. *Nanoscale Res. Lett.* **2008**, *3*, 468−472.
(20) Li, J. F.; Li, S. B.; Anema, J. R.; Yang, Z. L.; Huang, Y. F.; Ding, Y.; Wu, Y. F.; Zhou, X. S.; Wu, D. Y.; Ren, B.; Wang, Z. L.; Tian, Z. Q. *Appl. Spectrosc.* **2011**, *65*, 620−626.
(21) Lin, X. D.; Uzayisenga, V.; Li, J. F.; Fang, P. P.; Wu, D. Y.; Ren, B.; Tian, Z. Q. *J. Raman. Spectrosc.* **2012**, *43*, 40−45.
(22) Li, J. F.; Huang, Y. F.; Ding, Y.; Yang, Z. L.; Li, S. B.; Zhou, X. S.; Fan, F. R.; Zhang, W.; Zhou, Z. Y.; Wu, D. Y.; Ren, B.; Wang, Z. L.; Tian, Z. Q. *Nature* **2010**, *464*, 392−395.
(23) Rycenga, M.; Xia, X. H.; Moran, C. H.; Zhou, F.; Qin, D.; Li, Z. Y.; Xia, Y. N. *Angew. Chem., Int. Ed.* **2011**, *50*, 5473−5477.
(24) Tong, L. M.; Zhu, T.; Liu, Z. F. *Chem. Soc. Rev.* **2011**, *40*, 1296−1304.
(25) Rizia, B.; Nathaniel, K.; Grady; Naomi, J. H. *Small* **2008**, *4*, 1716−1722.
(26) Strobel, R.; Metz, H. J.; Pratsinis, S. E. *Chem. Mater.* **2008**, *20*, 6346−6351.
(27) Ehrmana, S. H.; Friedlander, S. K. *J. Mater. Res.* **1999**, *14*, 4551−4561.
(28) Liu, F. X.; Cao, Z. S.; Tang, C. J.; Chen, L.; Wang, Z. L. *ACS Nano* **2010**, *4*, 2643.